Solitonic in-gap modes in a superconductor-quantum antiferromagnet interface

J. L. Lado [1] and M. Sigrist[2]
[1]*Department of Applied Physics, Aalto University, 00076 Aalto, Espoo, Finland*
[2]*Institute for Theoretical Physics, ETH Zurich, 8093 Zurich, Switzerland*

(Received 17 February 2020; revised manuscript received 22 May 2020; accepted 28 May 2020; published 16 June 2020)

Bound states at interfaces between superconductors and other materials are a powerful tool to characterize the nature of the involved systems and to engineer elusive quantum excitations. In-gap excitations of conventional *s*-wave superconductors occur, for instance, at magnetic impurities with net magnetic moment breaking time-reversal symmetry. Here we show that interfaces between a superconductor and a quantum antiferromagnet can host robust in-gap excitations, without breaking time-reversal symmetry. We illustrate this phenomenon in a one-dimensional model system with an interface between a conventional *s*-wave superconductor and a one-dimensional Mott insulator described by a standard Hubbard model. This genuine many-body problem is solved exactly by employing a combination of kernel polynomial and tensor network techniques. We unveil the nature of such zero modes by showing that they can be adiabatically connected to solitonic solutions between a superconductor and a mean-field antiferromagnet. Our results put forward a new class of in-gap excitations between superconductors and a disordered quantum spin phase, including quantum spin-liquids, that can be relevant for a wider range of heterostructures.

DOI: 10.1103/PhysRevResearch.2.023347

I. INTRODUCTION

Topological modes emerging in condensed matter systems are among the most intriguing features in physics. Well-known examples are the electronic solitons in polyacetylene [1] or the Jackiw-Rebbi modes first introduced in high-energy theory [2]. In recent years the family of topological phases with extraordinary modes has been extended enormously to a multitude of novel systems with gapped bulk excitation spectra [3–5]. In almost all cases, such topological modes emerge in systems that can be described within the spectra of noninteracting electrons, whose single-particle Hamiltonians incorporate a nontrivial topology. Despite the large body of knowledge on topologically nontrivial excitations of noninteracting particles accumulated in recent years, the theoretical analysis of the many-body counterpart remains a formidable challenge.

Among the different in-gap states found in materials, those of superconductors have attracted special attention because they might provide valuable information about the nature of the superconducting phase, even if it is topologically trivial. On the one hand, a classical magnetic impurity (a static magnetic moment) gives rise to in-gap Yu-Shiba-Rusinov states in an *s*-wave superconductor, probing the vulnerability to the superconducting phase against time-reversal symmetry violation (spin polarization) [6–13]. On the other hand, in-gap states created by nonmagnetic impurities provide a strong signature for unconventional superconductivity [14–17].

Increasing complexity, for instance, through heterostructures connecting a superconductor to materials of various properties offers an attractive platform to create new emergent phases [18–20]. This is the basis for a plethora of proposals to engineer Majorana bound states [21], to explore unusual Andreev physics [22,22–25] and even to design higher-dimensional topological superconductors [26,27]. So far studies in this direction focused mainly on single-particle physics [3–5], e.g., system in which the excitation spectrum can be treated in a mean-field picture. Therefore, extending the scope to interface physics involving the strongly correlated electron regime with dominant quantum fluctuations represents a rich playground for new physics which is largely unexplored [28–32].

Here we demonstrate how solitonic in-gap modes can emerge at interfaces between a conventional superconductor and a quantum antiferromagnet without long-range order, both topologically trivial on their own. In particular, we show that time-reversal symmetry needs not to be broken and that these modes can be adiabatically connected with solitonic zero modes of the antiferromagnetically ordered phase violating time-reversal symmetry. In this way, we extend the set of situations where the composition of different materials can generate a nontrivial phase at interfaces. In particular, our results put forward a minimal model system where the interplay of superconductivity and quantum spin liquid physics gives rise to unconventional excitations.

The paper is organized as follows. In Sec. II we show the emergence of the solitonic zero mode and its robustness towards system parameters, by exactly solving the interacting model. In Sec. III we put forward a connection between

Published by the American Physical Society under the terms of the Creative Commons Attribution 4.0 International license. Further distribution of this work must maintain attribution to the author(s) and the published article's title, journal citation, and DOI.

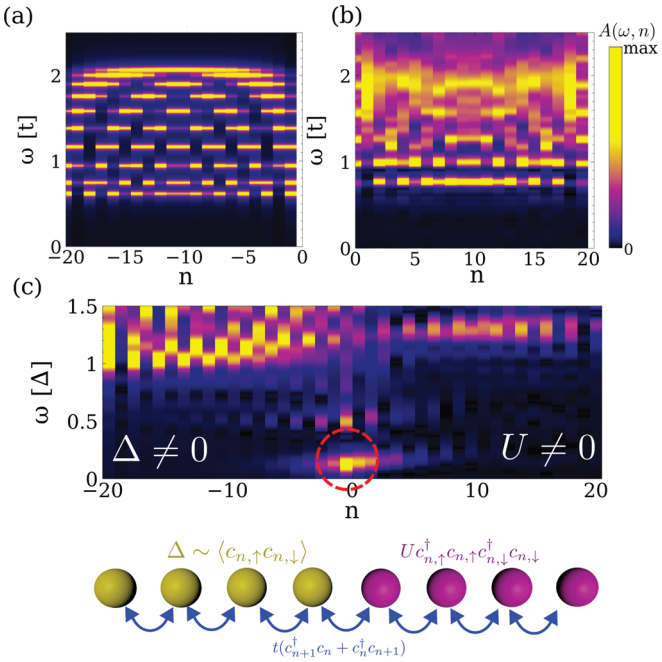

FIG. 1. (a) Spectral function of the superconductor, showing a gap up to the superconducting gap Δ, and of the quantum antiferromagnet (b), showing a gap on the order of the Hubbard U. Panel (c) shows the spectral function across the interface between the two systems, showing the emergence of in-gap modes at the interface in the absence of time reversal symmetry breaking. We use $\Delta = 0.6t$ and $U = 4t$. The inset below panel (c) shows a sketch of the model used to study the superconducting-antiferromagnetic interface.

the time-reversal symmetric interacting zero mode, and a solitonic zero mode in a noninteracting model with broken time-reversal symmetry. Finally, in Sec. IV we summarize our conclusions.

II. EMERGENCE OF A SOLITONIC MODE

We model our system by the following Hamiltonian of a one-dimensional chain, that allows us incorporate an interface between a conventional superconductor and a quantum antiferromagnet in the simplest way: $H = H_{\rm kin} + H_U + H_{\rm SC}$, where $H_{\rm kin}$ is the kinetic energy term in a tight-binding form

$$H_{\rm kin} = t\sum_{n,s}[c^\dagger_{n,s}c_{n+1,s} + c^\dagger_{n+1,s}c_{n,s}] + \sum_{n,s}\mu(n)c^\dagger_{n,s}c_{n,s}, \quad (1)$$

H_U is the Hubbard interaction term with a position dependent U

$$H_U = \sum_{n,s} U(n)c^\dagger_{n,\uparrow}c_{n,\uparrow}c^\dagger_{n,\downarrow}c_{n,\downarrow}, \quad (2)$$

and $H_{\rm SC}$ introduces conventional superconductivity in the mean-field formulation

$$H_{\rm SC} = \sum_n \Delta(n)[c_{n\uparrow}c_{n\downarrow} + c^\dagger_{n\downarrow}c^\dagger_{n\uparrow}]. \quad (3)$$

The heterostructure can be modeled by the parametrization $U(n) = [\tanh(n/W) + 1]U/2$, and $\Delta(n) = [-\tanh(n/W) + 1]\Delta/2$ locating the interface at $n = 0$ [Fig. 1(a)], and we take $W = 1$. The profile of $\mu(n)$ is chosen as $\mu(n) = -U(n)/2$ so that the system is half filled everywhere. Our calculations are performed in chains having 40 sites.

For the treatment of this genuine many-body Hamiltonian we employ the computational matrix product state formalism and, in particular, determine the local single-particle spectral function defined as

$$A(\omega, n) = \sum_s \langle GS|c^\dagger_{n,s}\delta(\omega - H + E_{GS})c_{n,s}|GS\rangle. \quad (4)$$

This dynamical correlation function can be computed for the whole frequency range by exploiting a kernel polynomial technique [33] implemented within the matrix product state formalism of ITensor [34,35]. The basic idea of the method consists of representing the function $A(n, \omega)$ in a complete functional basis expanded by N Chebyshev polynomials $T_k(\omega)$ as $A(\omega, n) = \frac{1}{\pi\sqrt{1-\omega^2}}(\mu_0 + 2\sum_{k=1}^N \mu_k T_k(\omega))$. The coefficients μ_k are obtained as $\mu_k = \langle GS|c^\dagger_n T_k(H)c_n|GS\rangle$ [36] that can be recursively computed through products of matrix product operators and matrix product states [33,37–39]. Note that for this algorithm the time evolution is not needed since we work from the beginning in frequency space.

The spectral function $A(n, \omega)$ shows the quasiparticle excitation gap in real space. Thus, it is instructive to consider first each subsystem of the model separately using our computational scheme for a system of finite length. For the uniform superconductor, $A(\omega, n)$ shows a quasiparticle gap [Fig. 1(a)]. The half-filled Hubbard chain with $U > 0$ is not magnetically ordered, but displays a Mott charge excitation gap as seen in Fig. 1(b) [40–42]. Note that the spatial dependence of the spectral functions in Figs. 1(a) and 1(b) is a finite-size effect induced by the open boundary conditions. It is also interesting to note that both systems are topologically trivial, lacking in-gap edge modes.

We turn now to the spatially resolved spectrum of a heterostructure connecting the two phases. As shown in Fig. 1(c), the system shows now in-gap excitations (the lowest one highlighted with the dashed red circle), which are clearly a feature connected with the interface ($n \approx 0$). Besides the previous in-gap mode, a second in-gap state at a higher energy can be observed at the interface in Fig. 1(c). In-gap states in an s-wave superconductor are usually attributed to static magnetic impurities, giving rise to the so-called Yu-Shiba-Rusinov states. In our case, however, time-reversal symmetry is conserved and there are no static moments despite the suppression of charge fluctuation on the Mott side ($n > 0$). Moreover, the dominant mode here is essentially pinned at zero, a feature that does not happen for generic Yu-Shiba-Rusinov states.

Let us now consider the properties of this interface excitation. First, we examine how the interface mode behaves for varying the model parameters Δ and U. In Fig. 2(a) the spectral function $A(\omega, n = 0)$ as function of Δ for fixed $U = 6t$ shows the evolution of the lowest mode toward $\omega = 0$ upon increasing Δ. With increasing Δ the two in-gap modes [red and blue dashed line in Fig. 2(a)] converge to stable in-gap energies, while the bulk superconducting gap increases (white dashed line, note the shift due to finite-size effects). Figures 2(b) to 2(d) display the U-dependence for fixed $\Delta = 0.4t$. In Fig. 2(b) we show how the charge fluctuations are

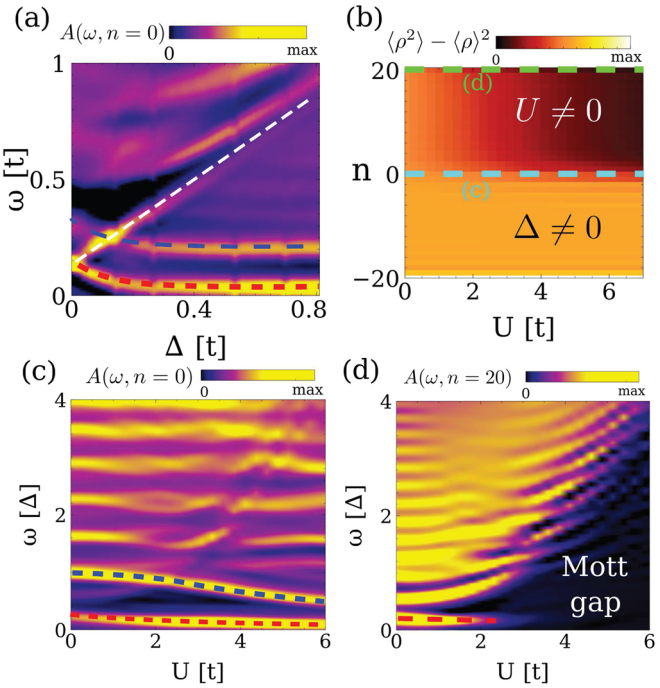

FIG. 2. (a) Evolution of the spectral function at the interface as a function of the superconducting pairing Δ, for the other half chain with finite U. Panels (b) (c), and (d) show the evolution as a function of U with the superconducting part at a fixed finite Δ. Panel (b) shows the spatially resolved charge fluctuation in (b), the spectral function at the interface in (c), and the spectral function in the quantum antiferromagnetic part in (d). We use $U = 6t$ for (a) and $\Delta = 0.4t$ for (b)–(d).

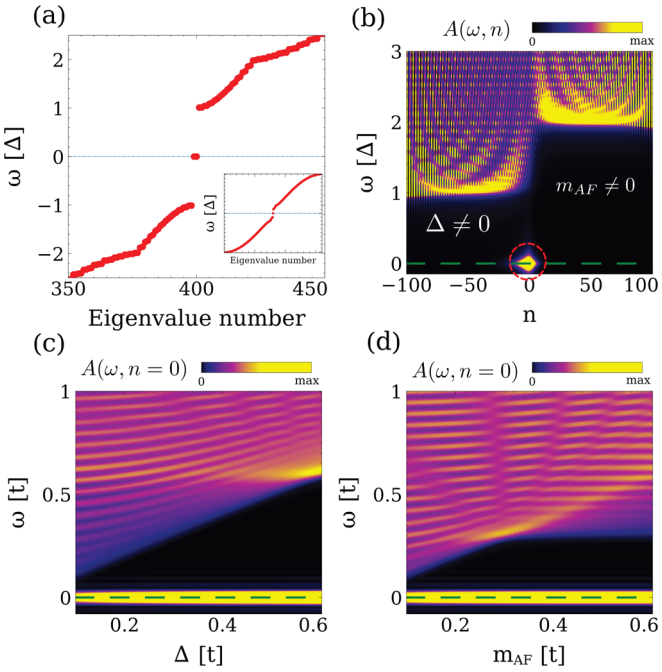

FIG. 3. (a) Bogoliubov de Gennes spectra of the superconductor-stagger antiferromagnet interface, showing the existence of a zero mode. Panel (b) shows the spatially resolved density of states $A(\omega, n)$ of the interface, showing that the zero mode is localized at the interface between the two systems. Panels (c), (d) show the evolution of the density of states at the interface as a function of the superconducting pairing Δ (c) and the antiferromagnetic stagger field m_{AF} (d), highlighting the robustness of the zero mode. We use for (a), (b) $m_{\mathrm{AF}} = 0.4t$ and $\Delta = 0.2t$, for (c) $m_{\mathrm{AF}} = 0.8t$ and for (d) $\Delta = 0.3t$. Note that the ω axis starts slightly below $\omega = 0$ for visibility, dark green dashed lines mark $\omega = 0$ in (b)–(d).

gradually suppressed in the Mott region, while they remain constant in the superconducting region. The zero-energy mode (red dashed line) also settles at the interface upon increasing U as shown in Fig. 2(c), and similar behavior happens with the next in-gap state (blue dashed line) [43]. For comparison, we observe that the low-energy modes progressively fade away in the interior of the Mott region when U is increased [see Fig. 2(d)].

III. ORIGIN OF THE SOLITONIC MODE

A further path to elucidate the character of the zero-energy modes runs via the using a mean-field antiferromagnetic phase for $n > 0$. We restrict to the single-particle description by replacing H_U by $H_{\mathrm{AF}} = \sum_n (-1)^n m_{\mathrm{AF}}(n)[c^\dagger_{n\uparrow}c_{n\uparrow} - c^\dagger_{n\downarrow}c_{n\downarrow}]$ with the spatial profile $m_{\mathrm{AF}}(n) = [1 + \tanh(n/W)]m_{\mathrm{AF}}/2$ and $\Delta(n) = [1 - \tanh(n/W)]\Delta/2$. The Hamiltonian for this inhomogeneous one-dimensional (1D) system can be easily solved numerically by means of a Bogoliubov de Gennes (BdG) scheme with the results displayed in Fig. 3. We find zero-energy modes within the gap in the sequence of eigenvalues [Fig. 3(a)] and can locate them clearly at the interface [Fig. 3(b)]. When changing the system parameters Δ for fixed $m_{\mathrm{AF}} = 0.8t$ [Fig. 3(c)] and m_{AF} for fixed $\Delta = 0.3t$ [Fig. 3(d)] we observed that this mode remains solidly at $\omega = 0$, which demonstrates clearly that this feature is not an effect of fine-tuning.

The nature of this interface mode can be easily explained with an analytical approach in the continuum limit of this model. For this purpose we choose a two-site unit cell adapted to the staggered moment (A and B sublattice) and rewrite the kinetic energy term in k-space

$$H(k) = \begin{pmatrix} 0 & 1 + e^{ik} \\ 1 + e^{-ik} & 0 \end{pmatrix}, \tag{5}$$

which near $k = \pi$ takes the form of a 1D Dirac equation with $H(p) = \tau_y p$, with τ_y the sublattice Pauli matrix. We now use $p = -i\partial_x$, introduced into the adapted H_{AF} and H_{SC} and turn to continuum variables $c_{2n} \to \psi_A(x)$, $c_{2n+1} \to \psi_B(x)$, $\Delta(n) \to \Delta(x)$, $m_{AF}(n) \to m_{AF}(x)$ defining the continuum 1D Hamiltonian

$$H = \sum_{s,\alpha,\beta} p\tau_y^{\alpha\beta}\psi^\dagger_{\alpha,s}\psi_{\beta,s} + \sum_{s,\alpha} m_{\mathrm{AF}}(x)\sigma_z^{ss}\psi^\dagger_{\alpha,s}\psi_{\alpha,s} + \sum_{\alpha} \Delta(x)[\psi_{\alpha,\uparrow}\psi_{\alpha,\downarrow} + \psi^\dagger_{\alpha,\downarrow}\psi^\dagger_{\alpha,\uparrow}]. \tag{6}$$

This Hamiltonian can be diagonalized defining the Nambu spinor $\Psi = (\psi_{A,\uparrow}, \psi_{B,\uparrow}, \psi^\dagger_{A,\downarrow}, \psi^\dagger_{B,\downarrow})$, for the sector of spin-up

electron/spin-down hole, where we obtain $H \sim \Psi^\dagger \mathcal{H} \Psi$ with

$$\mathcal{H} = \begin{pmatrix} m_{\rm AF}(x) & ip & \Delta(x) & 0 \\ -ip & -m_{\rm AF}(x) & 0 & \Delta(x) \\ \Delta(x) & 0 & m_{\rm AF}(x) & -ip \\ 0 & \Delta(x) & ip & -m_{\rm AF}(x) \end{pmatrix}. \quad (7)$$

The spectrum is obtained by BdG transformation. While both the superconductor and the antiferromagnet have an excitation gap, we find at the interface a zero-energy eigenvalue with an eigenoperator [2,44–46]

$$\Psi^\dagger = \tfrac{1}{2}[c^\dagger_{A,\uparrow} + c^\dagger_{B,\uparrow} - c_{A,\downarrow} + c_{B,\downarrow}] e^{\int_0^x [\Delta(x') - m_{\rm AF}(x')] dx'} \quad (8)$$

for $m_{\rm AF}(\infty) > 0$ [47]. Note that since Eq. (7) is a real differential equation, the solitonic zero-mode Eq. (8) has real coefficients. Note that for a given choice of $m_{\rm AF}$, only a single [48] zero mode exists. It is also worth to note that time-reversal symmetry Θ is not a symmetry of the interface. As a result, for the time-reversal counterpart of the previous system, the zero-mode excitation will be $\Theta\Psi^\dagger\Theta^{-1}$, different from $\Psi^\dagger$. Intuitively, the action of time-reversal symmetry is equivalent to switching between positive or negative magnetic moments. In the noninteracting Hamiltonian presented, the zero-energy mode can be derived analytically, yet an analogous approach is not available if we replace the mean field by a quantum antiferromagnet where the many-body nature of the system is important.

Although the many-body problem is challenging, we may connect with the previous solitonic mode by extending the many-body Hamiltonian with a staggered field on the Mott side, i.e., $H = H_{\rm kin} + H_U + H_{\rm SC} + H_{\rm AF}$. In this way, we introduce a static moment in addition to the quantum fluctuation. This model shall again be solved by our computational many-body scheme. The schematic result obtained is shown in Fig. 4(a) that shows that the two time-reversal related solutions found in the single-particle case, merge in the pure quantum limit yielding localized in-gap mode. The previous sketch captures only the single-particle charge excitations reflected in the correlator Eq. (4), whereas the many-body spectrum will show a continuum of states stemming from the gapless spinon modes of the quantum antiferromagnet. The transition from the quantum to the classical regime as the stagger magnetization is switched on can be directly observed in the expectation value of the local magnetic moment, as shown in Fig. 4(b).

We now verify the previous picture by examining the spectral function Eq. (4) at the interface, $n = 0$ [Fig. 4(c)] and at $n = 10$ inside the Mott region [Fig. 4(d)]. We can observe how the in-gap mode is present for $m_{\rm AF} = 0$ and gradually transforms into the zero-energy solitonic mode just described, while the spectrum within the Mott region remains gapped. Thus, the in-gap spectrum of the many-body system is adiabatically connected to a time-reversal symmetry breaking situation where the low-energy quantum fluctuations are progressively suppressed upon increasing $|m_{\rm AF}|$.

An interesting feature is the splitting of in-gap mode into two branches when $m_{\rm AF}$ is switched on, whereby only one branch evolves into the solitonic zero-energy mode, while second rises in energy and gradually loses weight. Moreover, it is also important to note that depending on the sign of $m_{\rm AF}$,

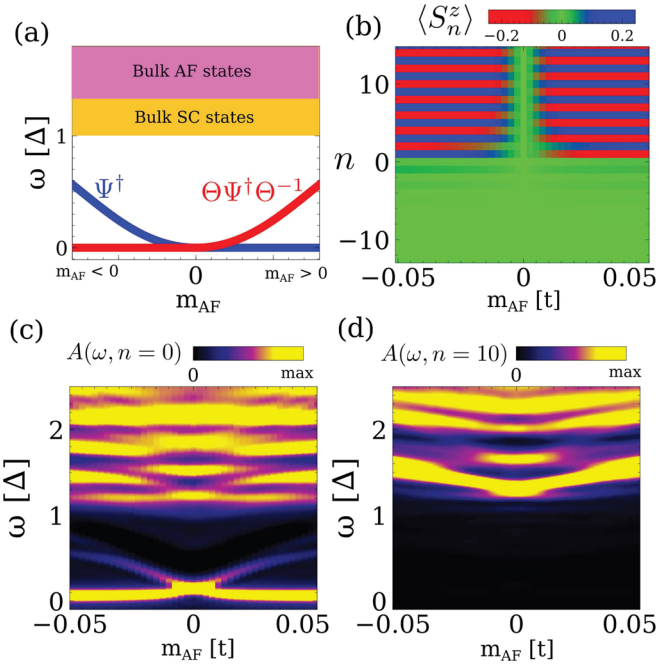

FIG. 4. (a) Sketch of the evolution of the charge excitation in the heterostructure, including the solitonic zero modes, as a function of the antiferromagnetic field $m_{\rm AF}$, showing that they become the in-gap excitations in the case of the quantum antiferromagnet. (b) Spatially resolved magnetization as a function of $m_{\rm AF}$. Panels (c), (d) show the spectral function at the interface (c) and in the middle of the antiferromagnetic region (d). We use $U = 6t$ and $\Delta = 0.6t$.

the low-energy mode will transform either into $\Psi^\dagger$ or into $\Theta\Psi^\dagger\Theta^{-1}$. In the quantum antiferromagnetic regime, the two modes coexist, such that there is a two-fold degeneracy for the in-gap mode at $m_{\rm AF} = 0$, whose energy needs not to lie at exactly zero.

Finally, we highlight two potential platforms to experimentally realize our proposal, bulk compounds showing quasi-1D chains and atomically engineered lattices. The first direction consists of creating an interface between a conventional superconductor and a compound hosting quasi-1D quantum antiferromagnets, such as $CuCl_2 - 2N(C_5D_5)$ [49], $KCuF_3$ [50], and Sr_2CuO_3 [51,52]. The second direction consists of exploiting atomic engineering with atomic scale microscopy [53] to create a quantum antiferromagnet [53–56] and putting it in contact with a superconductor [19].

IV. CONCLUSION

To summarize, we have put forward a minimal system consisting of a many-body quantum antiferromagnet and a conventional *s*-wave superconductor that host solitonic in-gap excitations. We unveiled the nature of those states, by showing that they can be adiabatically connected to solitonic states between a mean-field antiferromagnet and a superconductor, which resembles the Jackiw-Rebbi soliton. Our results put forward a minimal example in which solitonic modes appear between a quantum disordered magnet and a superconductor, providing a stepping stone towards the study of interfaces between superconductors and quantum spin liquids.

ACKNOWLEDGMENTS

M.S. is grateful for the financial support from the Swiss National Science Foundation (SNSF) through Division II (No. 163186 and 184739). J.L.L. acknowledges the computational resources provided by the Aalto Science-IT project.

APPENDIX A: ADIABATIC CONNECTION BETWEEN THE MEAN-FIELD AND MANY-BODY LIMIT

In this section we show alternative paths between a free and interacting limit, complementary to the results of Fig. 4 in the main text. We will analyze two cases. First, we connect the mean-field antiferromagnet and the interacting system, keeping the stagger magnetization. Second, we connect the mean-field antiferromagnet directly to the many-body time-reversal state. We elaborate on those two cases below.

First, we show in Fig. 5(a) the evolution of the interface spectral function defining a parametric Hamiltonian

$$H(U) = H_{\rm kin} + H_{\rm SC} + H_{\rm AF} + H_U(U), \tag{A1}$$

keeping a fixed $m_{\rm AF}$ and changing U. We observe that the solitonic mode exists in the whole range of this alternative parametric path. We note that time-reversal symmetry remains always broken due to the presence of a finite $m_{\rm AF}$.

Furthermore, to demonstrate the robustness of the adiabatic connection used in the main text, we show an alternative interpolation between the quantum and classical antiferromagnet. For this purpose, we now define the parametric Hamiltonian as

$$H(\lambda) = H_{\rm kin} + H_{\rm SC} + (1-\lambda)H_{\rm AF} + \lambda H_U, \tag{A2}$$

so that for $\lambda = 0$ the Hamiltonian becomes purely noninteracting (breaking time-reversal symmetry), whereas for $\lambda = 1$ the system becomes purely many-body (conserving time reversal symmetry). As it is observed in Fig. 5(b), the solitonic mode exists again in the whole parametric range, demonstrating its robustness.

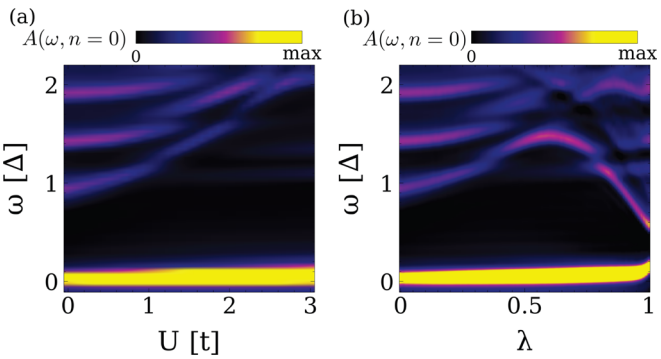

FIG. 5. (a) Evolution of the spectral function at the interface site for the Hamiltonian Eq. (A1), i.e., taking a constant $m_{\rm AF}$ and ramping up the value of the Hubbard U. Note that the whole path has broken time-reversal symmetry. Panel (b) shows the interface spectral function for the parametric path defined in Eq. (A2), where $\lambda = 0$ denotes the analytically solvable limit, and $\lambda = 1$ the quantum limit (with time-reversal symmetry). It is observed that the solitonic mode remains robust in both paths, keeping a finite bulk gap. We took $\Delta = 0.5t$ for (a), (b), $U = 5t$ for (b), and $m_{\rm AF} = 0.3t$ for (a), (b).

It is interesting to note that since the interface mode is not of topological origin, there is not a symmetry protected topological index associated with it. This is what allows us to connect smoothly the symmetry broken state, and the time-reversal symmetric many-body soliton. We highlight that along this path, the bulk charge gap of the antiferromagnet remains open, so that the evolution of solitonic mode can be clearly followed.

Finally, we note that although the emergence of in-gap states at interfaces between time-reversal symmetry broken states and superconductors is a generic feature [57] and has been shown also for antiferromagnetic interfaces [44–46,58,59]. However, in the present case we showed that a robust zero mode appears in the presence of time-reversal symmetry conservation, and therefore represents a case dramatically different from conventional Yu-Shiba-Rusinov states [57].

APPENDIX B: FINITE-SIZE SCALING

In this section we show that the interface solitonic excitation becomes independent of the length of the chain for large chain size.

We first focus on the effect of different lengths for the analytically solvable mean-field antiferromagnet. We first show in Fig. 6 the spectral function in the noninteracting limit for chains with $L = 40$ and $L = 80$ sites (besides the $L = 200$ case shown in the main text), highlighting that the zero mode does not change once chains are sufficiently long. This exemplifies that the interface mode for the $L = 200$ chain used in our main text is qualitatively analogous to the one for $L = 40$ and $L = 80$ of Fig. 6. We note that this case is easily solvable due to the single-particle nature of the system.

We now address the purely many-body quantum limit. In particular, we computed how the spectral function at the interface evolves with the size of the system as shown in Fig. 7. As it is observed, the solitonic zero mode remains robust for different system sizes [Figs. 7(a) and 7(c)]. In contrast, the second bound mode is sensitive to the size of the system, that slightly changes the Hamiltonian at the interface [Figs. 7(b) and 7(d)]. This result illustrates the robustness

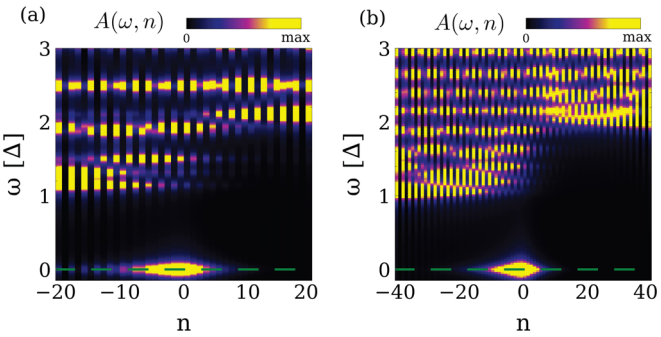

FIG. 6. Spectral function in the different sites, for an interface between a mean-field antiferromagnet and a superconductor, showing that zero mode is robust with respect to the size of the chain, 40 sites for (a) and 80 sites for (b). We took $m_{\rm AF} = 0.4t$ and $\Delta = 0.2t$.

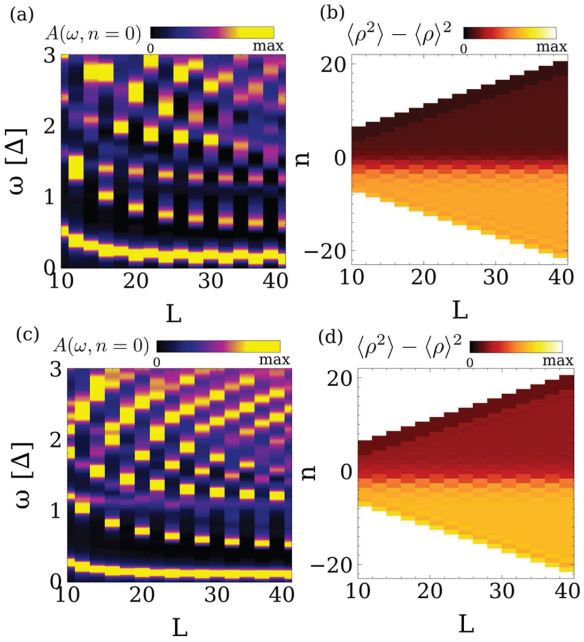

FIG. 7. (a), (c) Evolution of the spectral function at the interface as a function of the full length of the system L. (b), (d) Evolution of the density fluctuations in real space as a function of the chain length L. Panels (a), (b) are computed with $U = 6t$ and $\Delta = 0.4t$, whereas panels (c), (d) with $U = 4t$ and $\Delta = 0.6t$. It is observed that the solitonic zero mode becomes independent of the system size L for large L, and remains insensitive to the boundary conditions at the interface. In contrast, the second in-gap state is highly sensitive to the boundary conditions at the interface.

of the solitonic mode with respect to the system size, and justifies once more that with a $L = 40$ chain we reach already asymptotic results.

APPENDIX C: SPIN EXCITATIONS

In this section we address the interplay between the solitonic interface mode and the gapless spinon excitations of the antiferromagnet.

The solitonic excitation appears in the charge channel, in which both the superconductor and antiferromagnet are gaped. The quantum antiferromagnet is gapless only in the spin channel, where the gapless excitations are spinons. This suggests that the solitonic mode will be delocalized in the spin sector, yet localized in the charge sector. To illustrate this, we computed the dynamical response spin response, defined as

$$\mathcal{S}(\omega, n) = \langle GS|S^z_n \delta(\omega - H + E_{GS}) S^z_z|GS\rangle, \qquad \text{(C1)}$$

shown in Fig. 8. The solitonic mode cannot be easily distinguished in this channel, while only the gapless low-energy modes of the quantum antiferromagnet can be observed. This coexistence suggests than the spin sector of the solitonic mode becomes completely delocalized in the spinon bath, whereas the charge part remains confined to the interface, visible in the charge correlator shown in the main text.

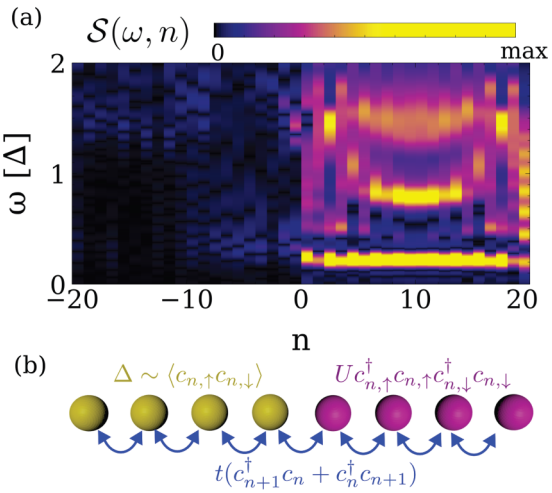

FIG. 8. (a) Dynamical spin response function $\mathcal{S}(\omega, n)$ of the superconducting-quantum antiferromagnet chain, as defined in Eq. (C1). It is observed that the quantum antiferromagnet shows excitations at low energies, which are associated with spinons of the Hubbard part. The solitonic excitation cannot be easily distinguished in this channel. Panel (b) shows a sketch of the model.

APPENDIX D: ROBUSTNESS OF THE SOLITON MODE TOWARDS PERTURBATIONS

In our main text we focused in the a minimal model for the sake of clarity. We now explicitly show that the details of the superconductor or the existence of additional perturbations do not matter for the existence of the solitonic mode. These results demonstrate that the zero mode survives a variety of perturbations present in a real system, and therefore can be experimentally observable.

We now elaborate on the different perturbations addressed, which are summarized below.

(1) Arbitrary doping in the superconductor [Eq. (D1)].
(2) Interface scattering [Eq. (D2)].
(3) Extended hopping [Eq. (D3)].
(4) Extended many-body interactions [Eq. (D4)].
(5) Anderson disorder [Eq. (D5)].
(6) Self-consistent treatment of the superconductor [Eq. (D6)].

In all those instances we observed the persistence of the many-body solitonic mode in our calculations (Fig. 9). We now elaborate on the results for the different terms considered.

The unperturbed Hamiltonian considered for the system is $H = H_{\rm kin} + H_U + H_{\rm SC}$, with the kinetic term $H_{\rm kin} = t\sum_{n,s}[c^\dagger_{n,s}c_{n+1,s} + c^\dagger_{n+1,s}c_{n,s}] + \sum_{n,s}\mu(n)c^\dagger_{n,s}c_{n,s}$, the local interactions of the form $H_U = \sum_{n,s} U(n) c^\dagger_{n,\uparrow}c_{n,\uparrow}c^\dagger_{n,\downarrow}c_{n,\downarrow}$, and the superconducting term of the form $H_{\rm SC} = \sum_n \Delta(n)[c_{n\uparrow}c_{n\downarrow} + c^\dagger_{n\downarrow}c^\dagger_{n\uparrow}]$ as considered in the main text. $\Delta(n)$ is defined to be nonzero in the superconductor, $U(n)$ to be nonzero in the quantum antiferromagnet, and $\mu(n)$ is a local on-site energy. In the following we will add a variety of perturbations to the previous Hamiltonian, and show that the zero mode remains present.

First [Fig. 9(a)], we consider the case of a superconductor with an arbitrary doping. For that sake we define a new term

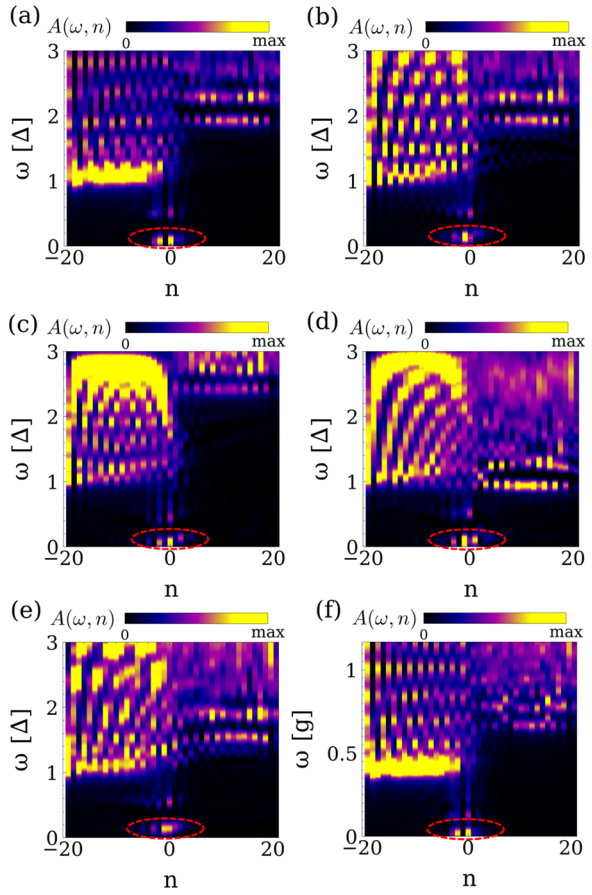

FIG. 9. Spectral function of the superconductor-quantum antiferromagnet system with different kinds of perturbations: (a) doping in the superconductor Eq. (D1), (b) interfacial potential scattering Eq. (D2), (c) extended hopping Eq. (D3), (d) extended interactions Eq. (D4), (e) Anderson disorder Eq. (D5), and (f) selfconsistent superconducting state Eq. (D6). It is observed that in all the instances the solitonic mode persists, demonstrating its robustness in realistic regimes. We took $\Delta = 0.6t$ in (a)–(e), $U = 5t$ in (a)–(f) and $N = 40$.

that acts as a chemical potential in the superconducting region

$$H_D = D \sum_{i\in \mathrm{SC},s} c^\dagger_{i,s} c_{i,s}, \tag{D1}$$

where $i \in$ SC denotes sum over the superconducting part, and we compute the spectral function for the Hamiltonian $\bar{H} = H + H_D$ where we take $D = 1.6t$. The result is shown in Fig. 9(a), and it is clearly observed that the interface zero mode remains robust. We verified that the same holds for arbitrary dopings of the superconductor. This robustness demonstrates that the existence of the zero mode is not related with the filling of the superconductor.

Second [Fig. 9(b)], we consider the existence of potential scattering in the interface, as would happen if there is an impurity at the interface between the antiferromagnet and the superconductor. The local scattering is implemented in terms of a local potential at the interface

$$H_{\mathrm{PS}} = w \sum_s c^\dagger_{0,s} c_{0,s} \tag{D2}$$

so that the total Hamiltonian is $\bar{H} = H + H_{\mathrm{PS}}$, and we took $w = 0.8t$. As it is observed in Fig. 9(b) the solitonic mode persists in the presence of potential scattering.

Third [Fig. 9(c)], we consider the existence of second neighbor coupling in our model

$$H_{NNN} = t_{NNN} \sum_{n,s} c^\dagger_{n,s} c_{n+2,s} + \mathrm{H.c.}, \tag{D3}$$

which breaks the bipartite nature of our model, and generalizes to realistic realizations where it is expected a finite second neighbor hopping. We take $t_{NNN} = 0.2t$, and compute the spectral function for the model $\bar{H} = H + H_{NNN}$, whose result is shown in Fig. 9(c). It is observed that the interface zero mode remains robust, even in the presence of extended hopping in the model. We also verified that the zero mode is also robust if the second neighbor hopping is included only in the superconductor or only in the quantum antiferromagnet.

Fourth [Fig. 9(d)], we consider the effect of nearest neighbor many-body interactions. In particular, we consider an additional interaction term of the form

$$H_V = V \sum_n \left(\sum_s c^\dagger_{n,s} c_{n,s} \right) \left(\sum_s c^\dagger_{n+1,s} c_{n+1,s} \right) \tag{D4}$$

that acts in the whole system, so that the total Hamiltonian is $\bar{H} = H + H_V$ and we take $V = 0.3t$. As it is observed in Fig. 9(d) the zero mode persists even in the presence of this additional interaction term. We also verified that the zero mode remains if the interaction is only considered in the superconducting or quantum antiferromagnetic part.

Fifth, we consider the effect of random Anderson disorder in the full system as

$$H_A = \sum_{n,s} \delta_n c^\dagger_{n,s} c_{n,s}, \tag{D5}$$

where δ_n is a random number for each site i between in the interval $[0, 0.4t]$. The total Hamiltonian considered $\bar{H} = H + H_A$, and as shown in Fig. 9(e) it is observed that the zero mode remains present even in the presence of disorder. We verified that the zero mode also remains if disorder is only included in the superconductor or antiferromagnet.

Finally, we consider the effect of a full self-consistent pairing. For this purpose, instead of imposing a superconducting pairing H_{SC}, we now start with an attractive interaction in the superconducting region of the form $H_g = -g \sum_{n\in \mathrm{SC},s} c^\dagger_{n,\uparrow} c_{n,\uparrow} c^\dagger_{n,\downarrow} c_{n,\downarrow}$ where $i \in$ SC denotes sum over the superconducting part. We perform a mean-field decoupling giving rise to

$$H_g^{\mathrm{MF}} = -g \sum_{n\in \mathrm{SC},s} \langle c^\dagger_{n,\uparrow} c^\dagger_{n,\downarrow} \rangle c_{n,\downarrow} c_{n,\uparrow} + \mathrm{H.c.}, \tag{D6}$$

so that the total Hamiltonian is $\bar{H} = H_{\mathrm{kin}} + H_U + H_D + H_g^{\mathrm{MF}}$. The normal term of the mean-field decoupling is reabsorbed in H_{kin}, and we take $g = 1.7t$. The term H_g^{MF} is computed self-consistently with the tensor network formalism. We note that this procedure treats the superconductor at the mean-field level, yielding a self-consistent superfluid density, whereas the antiferromagnet is still treated with the full many-body formalism. The results are shown in Fig. 9(f), and it is clearly

observed that the solitonic zero mode remains present when the superconducting term is computed self-consistently.

APPENDIX E: EXPERIMENTAL REALIZATION

In this section we present potential platforms to realize our model experimentally. Our proposal could be realized in two different ways, with bulk oxides showing quasi-1D chains or with atomically engineered lattices. We elaborate on this below.

We first address the proposal based on quasi-1D chains in a three-dimensional compound. This procedure consist on creating a junction between a conventional superconductor and a material hosting nearly decoupled 1D $S = 1/2$ antiferromagnetic chains, as shown in Fig. 10. Different compounds have been extensively studied showing quasi-1D physics associated to a strongly interacting Hubbard model, including $CuCl_2 - 2N(C_5D_5)$ [49], $KCuF_3$ [50], and Sr_2CuO_3 [51,52]. The interface should be perpendicular to the direction of the antiferromagnetic chains, as shown in Fig. 10(a). Those compounds were characterized as to realize an isotropic Heisenberg model. Taking an interface of any of those compounds with a conventional superconductor would lead to a realization of the scenario proposed in our paper. We note that although the superconductor is not three-dimensional, the emergence of the zero mode does not depend on the details of the superconducting part as elaborated in Appendix D.

We now address the proposal based on atomically engineered chains [53]. This realization is based on atomic-scale manipulation of individual atoms using an scanning tunneling microscope (STM), which allows to create atomically precise structures with specific atoms. These experimental developments allowed the realization, at the atomic level, a plethora of paradigmatic models, including one-dimensional quantum critical models [54], one-dimensional antiferromagnets [55], and atomic-scale ferromagnets with superconductors [19], among others [53]. The realization with this platform would require creating a one-dimensional antiferromagnetic Heisenberg chain, laterally contacted with a superconductor as shown in Fig. 10. We note that all the ingredients to realize this structure have been demonstrated, including quantum antiferromagnetism in $S = 1/2$ systems [56] and superconductivity in combination with in atomic-scale engineered chains [19].

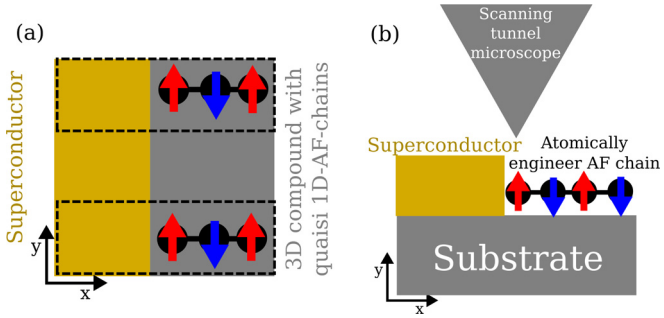

FIG. 10. (a) Sketch of an experimental realization of our proposal using a three-dimensional compound hosting quasi-1D AF chains. Panel (b) shows a sketch of a realization of our proposal using atomically engineered spin chains.

[1] W. P. Su, J. R. Schrieffer, and A. J. Heeger, Phys. Rev. Lett. **42**, 1698 (1979).
[2] R. Jackiw and C. Rebbi, Phys. Rev. D **13**, 3398 (1976).
[3] X.-L. Qi and S.-C. Zhang, Rev. Mod. Phys. **83**, 1057 (2011).
[4] M. Z. Hasan and C. L. Kane, Rev. Mod. Phys. **82**, 3045 (2010).
[5] Y. Ando and L. Fu, Annu. Rev. Condens. Matter Phys. **6**, 361 (2015).
[6] J. O. Island, R. Gaudenzi, J. de Bruijckere, E. Burzurí, C. Franco, M. Mas-Torrent, C. Rovira, J. Veciana, T. M. Klapwijk, R. Aguado, and H. S. J. van der Zant, Phys. Rev. Lett. **118**, 117001 (2017).
[7] D.-J. Choi, C. G. Fernández, E. Herrera, C. Rubio-Verdú, M. M. Ugeda, I. Guillamón, H. Suderow, J. I. Pascual, and N. Lorente, Phys. Rev. Lett. **120**, 167001 (2018).
[8] M. Ruby, F. Pientka, Y. Peng, F. von Oppen, B. W. Heinrich, and K. J. Franke, Phys. Rev. Lett. **115**, 087001 (2015).
[9] W. Chang, V. E. Manucharyan, T. S. Jespersen, J. Nygård, and C. M. Marcus, Phys. Rev. Lett. **110**, 217005 (2013).
[10] M. Ruby, Y. Peng, F. von Oppen, B. W. Heinrich, and K. J. Franke, Phys. Rev. Lett. **117**, 186801 (2016).
[11] M. Ruby, B. W. Heinrich, Y. Peng, F. von Oppen, and K. J. Franke, Phys. Rev. Lett. **120**, 156803 (2018).
[12] B. M. Andersen, K. Flensberg, V. Koerting, and J. Paaske, Phys. Rev. Lett. **107**, 256802 (2011).
[13] L. Cornils, A. Kamlapure, L. Zhou, S. Pradhan, A. A. Khajetoorians, J. Fransson, J. Wiebe, and R. Wiesendanger, Phys. Rev. Lett. **119**, 197002 (2017).
[14] A. I. Larkin, JETP Lett. **2**, 130 (1965).
[15] A. J. Millis, S. Sachdev, and C. M. Varma, Phys. Rev. B **37**, 4975 (1988).
[16] R. J. Radtke, K. Levin, H.-B. Schüttler, and M. R. Norman, Phys. Rev. B **48**, 653 (1993).
[17] A. P. Mackenzie, R. K. W. Haselwimmer, A. W. Tyler, G. G. Lonzarich, Y. Mori, S. Nishizaki, and Y. Maeno, Phys. Rev. Lett. **80**, 161 (1998).
[18] R. M. Lutchyn, J. D. Sau, and S. Das Sarma, Phys. Rev. Lett. **105**, 077001 (2010).
[19] S. Nadj-Perge, I. K. Drozdov, J. Li, H. Chen, S. Jeon, J. Seo, A. H. MacDonald, B. A. Bernevig, and A. Yazdani, Science **346**, 602 (2014).
[20] L. Fu and C. L. Kane, Phys. Rev. Lett. **100**, 096407 (2008).
[21] J. Alicea, Rep. Prog. Phys. **75**, 076501 (2012).
[22] Y. Tanaka, Y. Mizuno, T. Yokoyama, K. Yada, and M. Sato, Phys. Rev. Lett. **105**, 097002 (2010).
[23] F. Hübler, M. J. Wolf, T. Scherer, D. Wang, D. Beckmann, and H. V. Löhneysen, Phys. Rev. Lett. **109**, 087004 (2012).
[24] X.-J. Liu, Phys. Rev. Lett. **109**, 106404 (2012).
[25] Y. Tanaka and S. Kashiwaya, Phys. Rev. B **70**, 012507 (2004).

[26] F. Schindler, A. M. Cook, M. G. Vergniory, Z. Wang, S. S. P. Parkin, B. A. Bernevig, and T. Neupert, Sci. Adv. **4**, eaat0346 (2018).
[27] Z. Yan, Phys. Rev. B **100**, 205406 (2019).
[28] K. A. Al-Hassanieh, J. Rincón, G. Alvarez, and E. Dagotto, Phys. Rev. Lett. **114**, 066401 (2015).
[29] R. Thomale, S. Rachel, and P. Schmitteckert, Phys. Rev. B **88**, 161103(R) (2013).
[30] D. Sticlet, L. Seabra, F. Pollmann, and J. Cayssol, Phys. Rev. B **89**, 115430 (2014).
[31] A. E. Feiguin, S. R. White, and D. J. Scalapino, Phys. Rev. B **75**, 024505 (2007).
[32] A. Haim, A. Keselman, E. Berg, and Y. Oreg, Phys. Rev. B **89**, 220504(R) (2014).
[33] A. Weiße, G. Wellein, A. Alvermann, and H. Fehske, Rev. Mod. Phys. **78**, 275 (2006).
[34] ITensor Library (version 2.0.11), http://itensor.org.
[35] https://github.com/joselado/dmrgpy.
[36] The Hamiltonian must be scaled to the interval $(-1, 1)$ to perform the Chebyshev expansion.
[37] F. A. Wolf, I. P. McCulloch, O. Parcollet, and U. Schollwöck, Phys. Rev. B **90**, 115124 (2014).
[38] F. A. Wolf, J. A. Justiniano, I. P. McCulloch, and U. Schollwöck, Phys. Rev. B **91**, 115144 (2015).
[39] J. L. Lado and O. Zilberberg, Phys. Rev. Res. **1**, 033009 (2019).
[40] K. Penc, K. Hallberg, F. Mila, and H. Shiba, Phys. Rev. Lett. **77**, 1390 (1996).
[41] Z. Chen, X. Li, and T. K. Ng, Phys. Rev. Lett. **120**, 046401 (2018).
[42] M. Gulácsi and K. S. Bedell, Phys. Rev. Lett. **72**, 2765 (1994).
[43] This second in-gap mode is sensitive to the boundary conditions at the interface as discussed in the Appendix.
[44] P. San-Jose, J. L. Lado, R. Aguado, F. Guinea, and J. Fernández-Rossier, Phys. Rev. X **5**, 041042 (2015).
[45] J. L. Lado and M. Sigrist, Phys. Rev. Lett. **121**, 037002 (2018).
[46] A. L. R. Manesco, G. Weber, and D. Rodrigues, Phys. Rev. B **100**, 125411 (2019).
[47] For $m_{\mathrm{AF}}(\infty) < 0$, the m_{AF} in the exponent gets an additional minus sign to keep the wave function normalized.
[48] Note that this mode is not electron-hole symmetric.
[49] I. U. Heilmann, G. Shirane, Y. Endoh, R. J. Birgeneau, and S. L. Holt, Phys. Rev. B **18**, 3530 (1978).
[50] D. A. Tennant, T. G. Perring, R. A. Cowley, and S. E. Nagler, Phys. Rev. Lett. **70**, 4003 (1993).
[51] K. R. Thurber, A. W. Hunt, T. Imai, and F. C. Chou, Phys. Rev. Lett. **87**, 247202 (2001).
[52] N. Motoyama, H. Eisaki, and S. Uchida, Phys. Rev. Lett. **76**, 3212 (1996).
[53] D.-J. Choi, N. Lorente, J. Wiebe, K. von Bergmann, A. F. Otte, and A. J. Heinrich, Rev. Mod. Phys. **91**, 041001 (2019).
[54] R. Toskovic, R. van den Berg, A. Spinelli, I. S. Eliens, B. van den Toorn, B. Bryant, J.-S. Caux, and A. F. Otte, Nat. Phys. **12**, 656 (2016).
[55] S. Loth, S. Baumann, C. P. Lutz, D. M. Eigler, and A. J. Heinrich, Science **335**, 196 (2012).
[56] K. Yang, Y. Bae, W. Paul, F. D. Natterer, P. Willke, J. L. Lado, A. Ferrón, T. Choi, J. Fernández-Rossier, A. J. Heinrich, and C. P. Lutz, Phys. Rev. Lett. **119**, 227206 (2017).
[57] A. V. Balatsky, I. Vekhter, and J.-X. Zhu, Rev. Mod. Phys. **78**, 373 (2006).
[58] B. M. Andersen, I. V. Bobkova, P. J. Hirschfeld, and Y. S. Barash, Phys. Rev. B **72**, 184510 (2005).
[59] S. Zhen, H. Zhang, Q. Zhang, and Z. Dong, J. Supercond. Novel Magn. **32**, 1945 (2019).